Localized 5*f* antiferromagnetism in cubic UIn_3: ^{115}In-NMR/NQR study

Hironori Sakai,[1,*] Shinsaku Kambe,[1] Yo Tokunaga,[1] Hiroyuki Chudo,[1] Yoshifumi Tokiwa,[2,†] Dai Aoki,[2,‡] Yoshinori Haga,[1] Yoshichika Ōnuki,[1,2] and Hiroshi Yasuoka[1]

[1]*Advance Science Research Center, Japan Atomic Energy Agency, Tokai, Naka, Ibaraki 319-1195, Japan*

[2]*Graduate School of Science, Osaka University, Toyonaka, Osaka 560-0043, Japan*

(Received 31 October 2008; revised manuscript received 22 December 2008; published 24 March 2009)

^{115}In nuclear magnetic resonance (NMR) and nuclear quadrupole resonance (NQR) measurements have been performed on an antiferromagnet UIn_3 with the cubic $AuCu_3$-type structure. The NQR frequency (ν_Q) and Knight shift (K) of ^{115}In in UIn_3 have been estimated in the paramagnetic state from NMR experiments under applied field. The perpendicular component of transferred hyperfine coupling constant ($A_\perp$) has been deduced from scaled behavior of K to the static susceptibility (χ). Under zero field, the observation of the NQR spectrum has led to an estimated ν_Q of 11.8 MHz at 90 K. The temperature variation in the NQR relaxation rates ($1/T_1$) far above the Néel temperature $T_N=88$ K approaches a constant value, which indicates a localized nature for the 5*f* electrons in this system. On the other hand, in the antiferromagnetically ordered state at 4 K (well below T_N), the ^{115}In-NMR spectrum has been scanned over frequencies ranging from ~20 to ~70 MHz under zero applied field. From the analysis of the NMR spectrum, we propose that the most plausible direction of antiferromagnetic U moments may be ⟨110⟩ among the possible orientations of ⟨100⟩, ⟨110⟩, or ⟨111⟩.

DOI: 10.1103/PhysRevB.79.104426 PACS number(s): 75.25.+z, 75.30.−m, 76.30.−v

I. INTRODUCTION

The uranium intermetallic compounds UX_3 (X=Al,Ga,In,Tl,Si,Ge,Sn,Pb) with the cubic $AuCu_3$-type structure exhibit a wide variety of physical and electronic properties, ranging from enhanced Pauli paramagnetism (X=Al,Si,Ge,Sn) to antiferromagnetism (X=Ga,In,Tl,Pb). The compound USn_3 is known to be a heavy fermion system with a large electronic specific heat constant $\gamma \sim 170$ mJ/(K^2 mol),[1] which appears to be close to antiferromagnetism in phase space.[2] As for the paramagnets UX_3 (X=Al,Si,Ge), their Fermi surfaces have been studied using de Haas–van Alphen (dHvA) oscillations and are well accounted for by 5*f* itinerant band calculations.[3–5] Very recently, the heavy fermion state of USn_3 has been characterized in some detail with antiferromagnetic (AF) spin-fluctuation model for itinerant magnets based on ^{119}Sn nuclear magnetic resonance (NMR) measurements.[6] Thus, our understanding of the paramagnetic UX_3 series has been advancing steadily.

On the other hand, it is also very important to investigate the antiferromagnets in the UX_3 series, where much remains to be clarified. For example, UGa_3 orders antiferromagnetically at $T_{N1} \sim 67$ K with a magnetic propagation vector (1/2, 1/2, 1/2) (type-II AF structure), then it undergoes a second magnetic transition at $T_{N2} \sim 40$ K.[7–11] Although the antiferromagnetic structure between T_{N1} and T_{N2} has been determined to be type II, with ordered moments directed along ⟨110⟩ by a thorough ^{69,71}Ga NMR study,[12] little is known about what happens below T_{N2}. As for the antiferromagnets UIn_3, UTl_3 (type-II AF), and UPb_3 (type-I AF), the propagation vectors of the spin structures have been found by means of neutron diffraction measurements,[13,14] but the ordered moment orientations are still controversial.

In the present study, we have investigated the magnetic ordering in UIn_3, which is an antiferromagnet with T_N=88 K. As hydrostatic pressure is applied up to 9 GPa, T_N is found to increase monotonically to 127 K.[15] Single crystal specific heat data have yielded $\gamma \simeq 40$ mJ/(K^2 mol). Several pieces of Fermi surface with relatively large cyclotron masses have been found in the AF state by means of dHvA oscillations.[16] The electrical resistivity above T_N is nearly temperature independent at ~90 $\mu\Omega$ cm but decreases steeply below T_N.[16] The static susceptibility χ shows Curie-Weiss behavior well above T_N, with no measurable anisotropy. The effective moment μ_{eff} and the Weiss temperature Θ are estimated to be $3.25\mu_B$/U and −176 K, respectively.[16] This value of μ_{eff} is close to the free ion values for U^{3+} or U^{4+}, which suggests that the 5*f* electrons are localized in nature in the paramagnetic state.

As for the AF structure of UIn_3, powder sample neutron diffraction studies have revealed that the AF-ordered moment $\sim 1\mu_B$/U and that the AF propagation vector is (1/2, 1/2, 1/2).[13] In this material, while neutron diffraction methods can determine the periodicity of the AF-ordered moment arrangement, it is impossible with a powder sample to determine the moments orientation, owing to the cubic symmetry. For the latter purpose the neutron measurements must be performed on a single crystal with magnetic field and/or uniaxial pressure. Microscopic probes that detect hyperfine fields, such as muon spin rotation (μSR), Mössbauer effect, NMR, etc., may also be used for this purpose. However, previous μSR (Refs. 17–20) and Mössbauer[21] studies have proposed that a noncollinear 3*k* structure with moments along ⟨111⟩ direction occurs in UIn_3, which is incompatible with type-II AF structure having simple-cubic sublattice. A γ-γ perturbed-angular-correlation (PAC) study of UIn_3, which employs γ-ray spectroscopy, has examined possible moment directions of ⟨100⟩, ⟨110⟩, or ⟨111⟩ with type-II AF order. As a result of this symmetry analysis, ⟨110⟩ is suggested to be the likely direction, although they cannot deny the possibility of ⟨100⟩.[22]

In general, NMR is a good tool for microscopic investigation of magnetic structure, giving useful data on magnetic

ordering that is complimentary to other microscopic probes. In this paper we report ^{115}In NMR and nuclear quadrupole resonance (NQR) studies of UIn_3. First of all, we study the static and dynamic magnetic response of the paramagnetic state, reporting data for the Knight shift K from NMR measurements and relaxation rates $1/T_1$ from NQR measurements. Then, spin correlations in the paramagnetic state are discussed in terms of comparison with two related materials UGa_3 and USn_3. Finally, the most plausible orientation of magnetic moments in the AF state of UIn_3 is straightforwardly seen from our results to be $\langle 110 \rangle$, among the possibilities of $\langle 100 \rangle$, $\langle 110 \rangle$, or $\langle 111 \rangle$. Furthermore, from the experimental findings, we will discuss about the other possibilities of AF moments such as $\langle uvw \rangle$, $\langle 11w \rangle$, or $\langle uv0 \rangle$.

II. EXPERIMENTAL

Single crystals of UIn_3 grown by the indium-flux method were used for NMR/NQR measurements. Several single crystals were selected from the same batch as was used for electrical resistivity, magnetic susceptibility, specific heat, and dHvA measurements.[16] In order to increase the surface penetration of rf fields, a powder UIn_3 sample was prepared by crushing the single crystals carefully. The powder was mixed with paraffin to insulate the surface of each particle and to prevent oxidation and decomposition. These procedures were performed in an inert-gas atmosphere. The mixed powder was loaded into a capsule made of polyimide film and was inserted into the rf coil of the NMR probe.

^{115}In NMR/NQR measurements were carried out using a phase-coherent pulsed spectrometer. Field-swept NMR spectra were obtained at constant frequency $\nu_L = 77.7$ MHz by accumulation of spin-echo signals at each step of applied field. Frequency-swept spectra under zero applied field were taken by tuning the rf network at each point.

The observed ^{115}In nuclei have a natural abundance of 95.72% and nuclear spin quantum number $I=9/2$. The nuclear gyromagnetic ratio for ^{115}In is $\gamma_N/2\pi = 0.93301$ MHz/kOe. In conventional notation, the NQR frequency ν_Q is defined as $\nu_Q \equiv \frac{3e^2qQ}{2I(2I-1)h}$, where eQ is the nuclear quadrupole moment and $eq \equiv V_{ZZ}$ is the principal component of the electric field gradient (EFG) tensor.

The nuclear spin-lattice relaxation time T_1 was measured using the inversion-recovery method. Values of NQR relaxation rates $1/T_1$ were obtained from fits to the following recovery function of nuclear magnetization

$$\frac{M(\infty)-M(t)}{M(\infty)} \propto \left\{ \frac{4}{33}\exp\left(-\frac{3t}{T_1}\right) + \frac{80}{143}\exp\left(-\frac{10t}{T_1}\right) + \frac{49}{165}\exp\left(-\frac{21t}{T_1}\right) + \frac{16}{715}\exp\left(-\frac{36t}{T_1}\right) \right\} \quad (1)$$

for the $4\nu_Q$-NQR line.[23]

III. RESULTS

The crystal structure of UIn_3 is shown in Fig. 1. The U sites have cubic local symmetry, whereas the In sites are tetragonal. The asymmetry parameter of EFG is $\eta=0$, and the local principal axis of the EFG for each In site (as denoted as $\boldsymbol{n}$ in Fig. 1) is perpendicular to the plane of the four nearest-neighbor U atoms. In terms of the local In site coordinates, the angle θ between the applied field (paramagnetic state)/hyperfine field (ordered state) is defined for the following NMR/NQR analysis. Hyperfine parameters, i.e., Knight shift K and nuclear quadrupole frequency ν_Q for ^{115}In, are derived from NMR spectra as shown in Fig. 2.

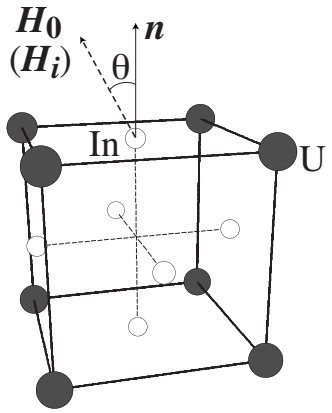

FIG. 1. Crystal structure of UIn_3 with the cubic $AuCu_3$-type structure. $\boldsymbol{n}$ indicates the local symmetry axis at the In site. The applied field H_0 (or hyperfine field H_i) is denoted by a dashed arrow.

If the Knight shift tensor is isotropic or $K \ll 1$, a typical NMR powder pattern with axial symmetry with $I=9/2$ will consist of a center line and eight first-order quadrupolar singularities. In addition, a small amount of splitting may occur in the center line due to the second-order quadrupolar terms. As seen in Fig. 2, the observed NMR spectra at 100 K

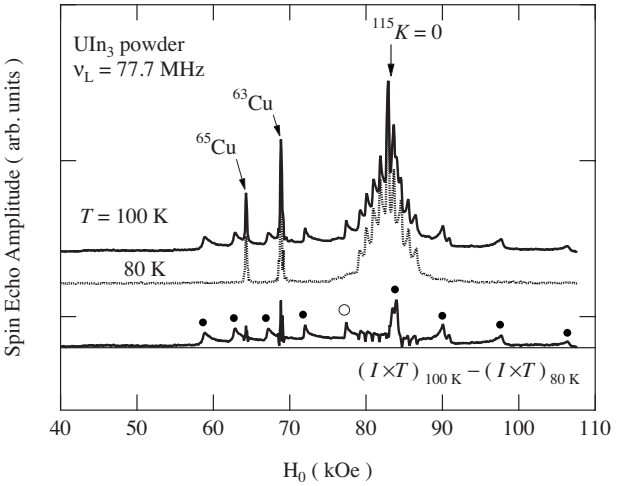

FIG. 2. Field-swept NMR spectra at a constant frequency $\nu_L = 77.7$ MHz, taken at 100 K (above T_N) and 80 K (below T_N) for ^{115}In in a powder sample of UIn_3. The difference between the spectra at 100 and 80 K is also shown (bottom tracing). The satellite singularities from the UIn_3 sample are marked by closed circles and the center-line singularity is also denoted by an open circle. The ^{63,65}Cu signals from the rf coil and the $K=0$ position for ^{115}In are denoted by arrows.

(above T_N) shows a superposition of two typical powder patterns, that is, one (here, tagged as spectrum I) has large intervals between satellites and another (tagged as spectrum II) has much smaller intervals. At $T=80$ K (below T_N), spectrum II remains as it does at $T=100$ K, while spectrum I disappears entirely. For more clarity, the difference between the $T=100$ and 80 K spectra is plotted in Fig. 2 (bottom trace). Spectrum I disappears below T_N because of spectral broadening by internal fields in the AF state and/or due to shortening of nuclear spin-spin relaxation time T_2. On the other hand, spectrum II remains with little change at the same position down to 4 K. The intervals between satellite singularities for spectrum II are $\nu_Q \sim 1.7$ MHz. This is close to the reported value $\nu_Q \sim 1.9$ MHz in indium metal.[24] Such extrinsic ^{115}In signals are attributed to indium metal from residual In flux and/or small decompositions of the sample. Thus, the nine intrinsic peaks (spectrum I) seen clearly in the bottom line are ascribed to the In sites of the sample.

From spectrum I, the center-line singularity, as denoted by open circle in Fig. 2, is found to depart from the $K=0$ position. It is noted here that this singularity corresponds to $\theta=90°$ from the principal EFG axis of the In sites and that the other center-line singularity at ($\theta=41.8°$) is veiled by the free indium metal spectrum II. ν_Q is estimated from the observed intervals to be about 11.8 MHz at 100 K. Since such a large ν_Q causes a second-order center-line shift, a correction should be made for this in the estimate of K. This second-order center-line shift $\Delta H_{\theta=90°}$ can be approximated by $-\frac{3\nu_Q^2}{2\nu_L}(\frac{\gamma_N}{2\pi})^{-1}=-2.88$ kOe at 100 K.

Figure 3(a) shows temperature dependence of the perpendicular component of shift $K_\perp$ ($\theta=90°$), which is estimated with corrections for the second-order quadrupolar shift using ν_Q values obtained from NQR experiments as shown below. $K_\perp$ and the static susceptibility χ both show a broad maximum around 100 K and then decrease gradually as temperature increases. To evaluate the transferred hyperfine coupling constant, we plot $K_\perp$ versus χ with temperature as an implicit parameter as shown in Fig. 3(b). A good linear relation between $K_\perp$ and χ is found, and the intercept at $\chi \to 0$ is near to $K=0$. This result indicates that K represents a transferred hyperfine field from the U moments. From the slope of the latter plot the perpendicular hyperfine coupling is estimated to be $A_\perp=54$ kOe/μ_B, similar to the value 59 kOe/μ_B reported for Sn sites in USn_3 from ^{119}Sn NMR.[6]

In recent empirical analyses, K-χ bending anomalies are found to occur widely in heavy fermion systems.[25] This presumably has to do with the condensation of heavy fermion liquids at low temperatures. Alternatively, such K-χ bending has also been explained by thermal depopulation of crystal electric field (CEF) levels.[26,27] The observed linear K-χ behavior which we find for UIn_3 suggests rather localized character for the 5*f* electrons without the heavy fermion condensation and/or a larger separation between ground and excited CEF levels.

Next, NQR signals for ^{115}In under zero applied field have been detected using the same powder sample. Figure 4 shows the NQR lines assigned to ^{115}In at 295 K. As seen in Fig. 4, the four lines at the frequencies of ν_Q, $2\nu_Q$, $3\nu_Q$, and $4\nu_Q$ are observed, which correspond to the four transitions

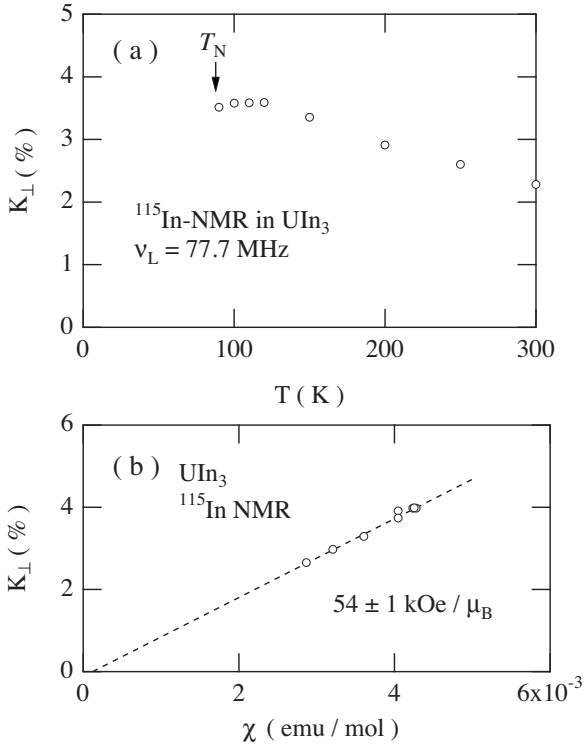

FIG. 3. (a) Temperature dependence of Knight shift $K_\perp$ for ^{115}In in the paramagnetic state of UIn_3. The values of $K_\perp$ are corrected for the second-order quadrupole shift. (b) The plot of $K_\perp$ against the static susceptibility χ along the *a* axis with temperature as an implicit parameter.

$\pm m \leftrightarrow \pm(m+1)$, where $m=\frac{1}{2}$, $\frac{3}{2}$, $\frac{5}{2}$, and $\frac{7}{2}$. The full widths at half maximum of the ν_Q and $4\nu_Q$ lines are about 150 and 400 kHz, respectively. Relatively narrow NQR lines indicate a good quality sample, i.e., there are relatively few lattice defects and/or magnetic impurities. The observed NQR frequencies for ^{115}In are very nearly equal to estimated frequencies obtained from the NMR results. This result assures us that the analyses of the NMR spectra are valid.

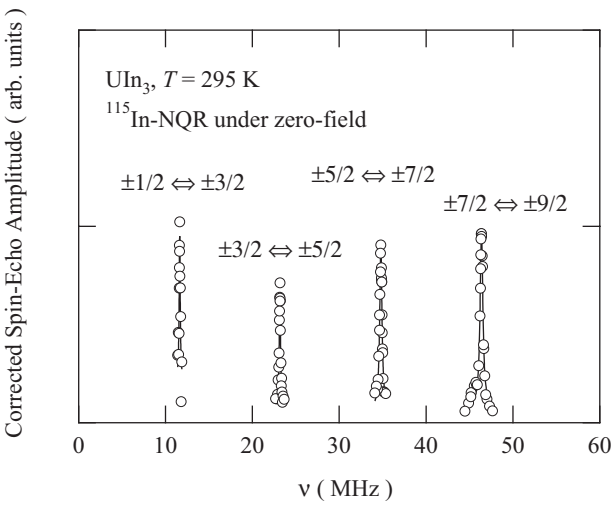

FIG. 4. ^{115}In NQR spectrum obtained at 295 K (paramagnetic state) under zero field.

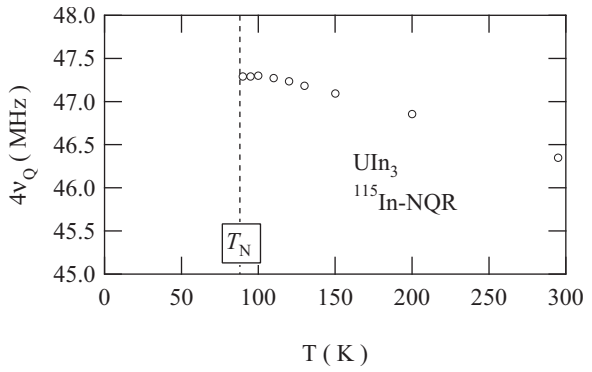

FIG. 5. Temperature dependence of $4\nu_Q$ for ^{115}In in the paramagnetic state of UIn_3.

In Fig. 5, the temperature dependence of the $4\nu_Q$ frequency is shown for the paramagnetic state of UIn_3. ν_Q gradually increases from 11.6 MHz at 295 K to 11.8 MHz at 90 K as temperature decreases toward T_N. Such a temperature dependence for ν_Q is often seen in paramagnetic metals. We also note the variation in NQR signal intensity as T decreases from well above T_N toward T_N. The signal intensity gradually becomes weaker, eventually becoming undetectable near T_N at frequencies around $4\nu_Q$. This diminishing of NQR signals just above T_N is a result of critical slowing down of AF fluctuations, as seen in Fig. 7. On the other hand, the vanishing of NQR signals just below T_N may be due to the onset of internal fields, i.e., the whole spectrum becomes spread out over a wide frequency range. This is similar to the disappearance of spectrum I just below T_N in the NMR scan.

However, as temperature decreases well below T_N, ^{115}In NMR signals under zero applied field reappear over a wide frequency range. These correspond to the development of internal fields with the AF ordering. The frequency-swept ^{115}In AFNMR spectrum under zero field at 4 K shows a complicated multivalley structure, as shown in Fig. 6. Here, the experimental data are divided by the square of local frequencies in order to extract relative transition probabilities between nuclear spin energy levels, whereas the so-called T_2 correction is not applied since the nuclear spin-spin relaxation time T_2 for each peak cannot be determined accurately. As seen in Fig. 6, the ^{115}In NMR spectrum in the AF state extends over a wide range of frequency, owing to large internal field splittings compared with the quadrupole interaction. We use this spectrum to discuss the AF structure in Sec. IV B.

Figure 7 shows the temperature dependence of NQR relaxation rates $1/T_1$ taken on the $4\nu_Q$ line in the paramagnetic state of UIn_3. In this figure, the $1/T_1$ vs T plots for the related materials USn_3 and UGa_3 are also superimposed for the comparison in Sec. IV A. As for UIn_3, well above T_N, constant behavior of $1/T_1$ is observed, which is related to the localized nature of $5f$ electrons in UIn_3. Below $\sim$100 K, an increase in $1/T_1$ due to critical slowing down is seen.

Next, we consider the hyperfine form factor for the ligand sites of UIn_3. The spin-lattice relaxation for this system may be expressed as[29]

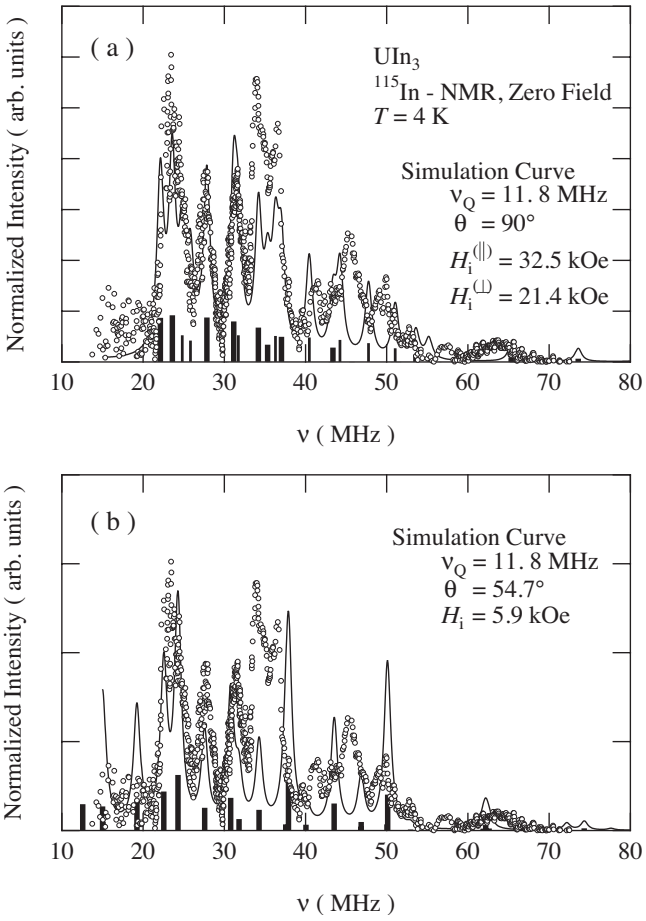

FIG. 6. Experimental frequency-swept NMR spectrum under zero applied field at 4 K (circles ○) and numerical simulations assuming the directions of the U moments are (a) ⟨110⟩ and (b) ⟨111⟩ (see text in Sec. IV B for the details). The solid curves are the convolutions of calculated transition lines with a Gaussian of natural width. Thick and thin lines denote the frequencies and intensities of transitions between nuclear spin energy levels at the In sites.

$$(1/T_1T)_{\mathrm{NQR}} \propto \sum_{\boldsymbol{q}} |A_\perp(\boldsymbol{q})|^2 \chi''_\perp(\boldsymbol{q},\omega_n) \simeq |A_\perp|^2 \sum_{\boldsymbol{q}} f^2(\boldsymbol{q}) \chi''_\perp(\boldsymbol{q},\omega_n), \tag{2}$$

where $A_\perp(\boldsymbol{q})$ is the component of $\boldsymbol{q}$-dependent hyperfine coupling perpendicular to the principal axis of the EFG, $\chi''_\perp(\boldsymbol{q},\omega_n)$ is the imaginary part of the dynamical susceptibility component perpendicular to the EFG axis, and $f^2(\boldsymbol{q})$ is the hyperfine form factor of the In sites, defined as $f^2(\boldsymbol{q}) \equiv |A_\perp(\boldsymbol{q})|^2/|A_\perp|^2$. Then, in this case,

$$f^2(\boldsymbol{q}) = 16\cos^2\left(\frac{q_x a}{2}\right)\cos^2\left(\frac{q_y a}{2}\right) \tag{3}$$

can be calculated from the local geometry of the sites. From Eq. (3) we see that $f^2(\boldsymbol{q})$ vanishes at the AF-$\boldsymbol{Q}$ $=(\pi/a,\pi/a,\pi/a)$, i.e., AF fluctuations are filtered out of NQR relaxation rates to some extent.

So, the observation of critical behavior in $1/T_1$ data may mean that the breadth of AF fluctuation peak on $\chi''(\boldsymbol{q},\omega)$

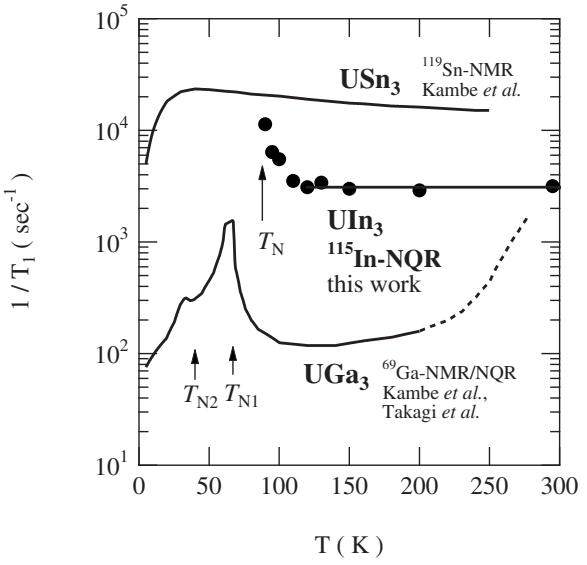

FIG. 7. Temperature dependence of $1/T_1$ in UX_3 (X=Ga,Sn,In). The NMR data for USn_3 are taken from Ref. 6, and the data for UGa_3 are from Refs. 12 and 28. In the case of UGa_3, the upturn of $1/T_1$ above ~200 K (broken line) is mainly due to nuclear quadrupolar anomaly (Ref. 28).

extends beyond the filtering effect of the $f^2(\boldsymbol{q})$ at $\boldsymbol{Q}$. In addition to this diagonal component, as discussed in Sec. IV B, we have found that off-diagonal transferred hyperfine fields also exist on the In sites, which cause the vertically transferred hyperfine fields from the nearest-neighboring U moments in the AF-ordered state. Therefore, this critical increase in $1/T_1$ near T_N may be arising partially from this off-diagonal component.

IV. DISCUSSION

A. Paramagnetic state of UIn_3

Above about 100 K the NQR T_1 values for ^{115}In are very nearly constant. Such a constant T_1 behavior in the high temperature range appears to reflect localized moment fluctuations for this system. Assuming the simple case of exchange-coupled localized moments, the exchange frequency ω_{ex} may be estimated from the measured Curie-Weiss temperature Θ taken from data for the uniform susceptibility,[29]

$$(\hbar\omega_{ex})^2 = (k_B\Theta)^2 \frac{3g_J}{z|g_J-1|^3 J(J+1)}, \tag{4}$$

where z is the number of nearest-neighbor magnetic ions (in this case, z=6 is adopted) and g_J is the Landé g factor. Using J=4 and $g_J=\frac{4}{5}$ for tetravalent U^{4+} ($5f^2$) or using $J=\frac{9}{2}$ and $g_J=\frac{8}{11}$ for trivalent U^{3+} ($5f^3$), ω_{ex} is estimated to be 1.9×10^{13} or 3.6×10^{13} s^{-1}, respectively. It should be noted here that the effective moment for UIn_3, which is estimated from the susceptibility,[16] is close to that of free-ionic values for U^{3+} or U^{4+}.

T_1 is then estimated assuming an isotropic hyperfine coupling constant A_{iso},

$$(1/T_1)_{limit} = \sqrt{2\pi}\left(\frac{\gamma_N g_J \mu_B A_{iso}}{z'}\right)^2 \frac{z'J(J+1)}{3\omega_{ex}}, \tag{5}$$

where z' is the number of magnetic ions coupling to the ligand nucleus (z'=4) and $A_{iso}^2 \simeq (A_\perp)^2$ is used. It is noted that hyperfine anisotropy for the related material USn_3 is found to be small. Then $(1/T_1)_{limit}$ is estimated to be 7.4×10^3 s^{-1} for U^{4+} or 1.4×10^4 s^{-1} for U^{3+}. In fact, the experimental values are very close to these exchange fluctuation limits, indicating localized character for this system.

For comparison with the related materials USn_3 and UGa_3, which have the same crystal structure, the temperature dependence of the relaxation rate $1/T_1$ is shown in Fig. 7. Here, USn_3 is a typical heavy fermion system, and UGa_3 can be categorized as an itinerant 5*f* AF material. The estimated values of $(1/T_1)_{limit}$ for each compound are listed in Table I, for which values were deduced assuming U^{4+} or U^{3+}. In the case of UGa_3, instead of Θ, T_{N1} has been adopted for the estimation of $(1/T_1)_{limit}$ since χ does not exhibit Curie-Weiss behavior in the paramagnetic region.

As shown in Fig. 7, USn_3 also shows nearly constant $1/T_1$ behavior at high temperatures, although Korringa behavior ($1/T_1 \propto T$) is seen below about 30 K, which corresponds to the formation of a strongly correlated Fermi liquid state. The constant behavior and relatively large values of $1/T_1$ in the heavy fermion material USn_3 indicate that this system may

TABLE I. Experimental and estimated values of $1/T_1$. The estimates of $1/T_1$ have been deduced on the basis of localized 5*f* moments for UX_3 (X=In,Ga,Sn) (see text). The experimental data for $1/T_1$ were taken at $T\sim200-300$ K for ^{115}In in UIn_3, ^{119}Sn in USn_3, and ^{69}Ga in UGa_3, as shown in Fig. 7. The Néel temperature (T_N) and Weiss temperature (Θ) are also listed.

	T_N (K)	Θ (K)	$(T_1^{-1})_{exp}$ (s^{-1})	$(T_1^{-1})_{limit}$ (s^{-1})	$(T_1^{-1})_{exp}/(T_1^{-1})_{limit}$
UIn_3	88	−176	3.1×10^3	7.4×10^3 (U^{4+})	4×10^{-1}
				1.4×10^4 (U^{3+})	2×10^{-1}
USn_3		−58	1.5×10^4	1.0×10^5 (U^{4+})	2×10^{-1}
				1.9×10^5 (U^{3+})	8×10^{-2}
UGa_3	66	[a]	2.0×10^2	1.3×10^5 (U^{4+})	2×10^{-3}
	($T_{N2}\sim40$)			2.4×10^5 (U^{3+})	8×10^{-4}

[a]The magnetic susceptibility does not show a Curie-Weiss-type behavior in the paramagnetic state.

border on $5f$ localization, although measured values of $1/T_1$ are about 1 order magnitude smaller than estimates of $(1/T_1)_{\text{limit}}$.

On the other hand, $1/T_1$ around 200 K in the paramagnetic state of UGa_3 reach only to 0.08%–0.2% of $(1/T_1)_{\text{limit}}$, indicating that $5f$ electrons in UGa_3 are still itinerant. It should be noted that $1/T_1$ increases anomalously above about 200 K, exhibiting quadrupolar anomalies as well,[28] which may or may not be related to the localization of $5f$ electrons.

Thus, the experimental values of $1/T_1$ in UIn_3 are found to be closest to the $(1/T_1)_{\text{limit}}$ among these materials. This suggests that $5f$ electrons have a localized character in the paramagnetic state of UIn_3.

B. AF-ordered state of UIn_3

As noted in Sec. I, neutron diffraction experiments[13] showed that UIn_3 exhibits type-II AF order with AF propagation vector (1/2, 1/2, 1/2). Moreover, since UIn_3 clearly exhibits localized character as discussed in Sec. IV A, the ordered U moment (μ_o) on each site is equal, of which amplitude has been determined by neutron diffraction to be about $1\mu_B$.[13] Therefore, only the orientation of μ_o remains open to question. It should be noted that the previously proposed $3k$ structure in UIn_3 was assumed on the type-I AF order with $\boldsymbol{k}=(1/2,0,0)$,[17–21] which is inconsistent with the type-II AF propagation vector determined by the neutron experiment. In addition, multi-k structure cannot appear in the case of AF $\mathbf{k}=(1/2,1/2,1/2)$ having a simple-cubic sublattice.

Generally, in cubic materials transferred hyperfine fields often cancel out at ligand sites, owing to the AF symmetry of the magnetic moments. However, as shown in Fig. 6, nonzero hyperfine fields have been observed at In sites in UIn_3 at 4 K, i.e., well below T_N. This may come from moments induced via anisotropic p-f hybridization, for which the hyperfine tensor is difficult to determine at present. However, Demuynck *et al.*[22] demonstrated that possible directions for induced X-site hyperfine fields in cubic UX_3 can be limited by symmetry analysis, regardless of the hyperfine mechanism. Following their analysis, we examine the three possibilities of $\mu_o \| \langle 100 \rangle$, $\| \langle 110 \rangle$, and $\| \langle 111 \rangle$, for the case of UIn_3 with a type-II AF structure, as illustrated in Fig. 8.

In the case of $\mu_o \| \langle 100 \rangle$, two In sites can occur that are magnetically distinguishable. As illustrated in Fig. 8(a), no induced fields can occur at one third of the In sites, and fields perpendicular to the direction of μ_o can appear at the rest of the In sites. Similarly, for the case of $\mu_o \| \langle 110 \rangle$, on one third of the In sites a hyperfine field $H_i^{(\|)}$ is induced parallel to μ_o, and a field $H_i^{(\perp)}$, perpendicular to μ_o, on the remaining two thirds. Both fields $H_i^{(\|,\perp)}$ lie in the local plane of the In sites, so in EFG coordinates the local field angles θ are 90°. In the case of $\mu_o \| \langle 111 \rangle$, all the In sites feel the unique H_i with the arbitrary angle of θ.

On the basis of the above considerations, we discuss possible orientation for μ_o from our experimental results. First, the possibility of $\mu_o \| \langle 100 \rangle$ is eliminated easily. If no induced hyperfine field could exist at one third of In sites, NQR signals would remain in the AF state. No such NQR signals observed below T_N, as noted in Sec. III. The remaining two possibilities are examined by the comparison of the experimental results with simulated curves, as shown in Fig. 6.

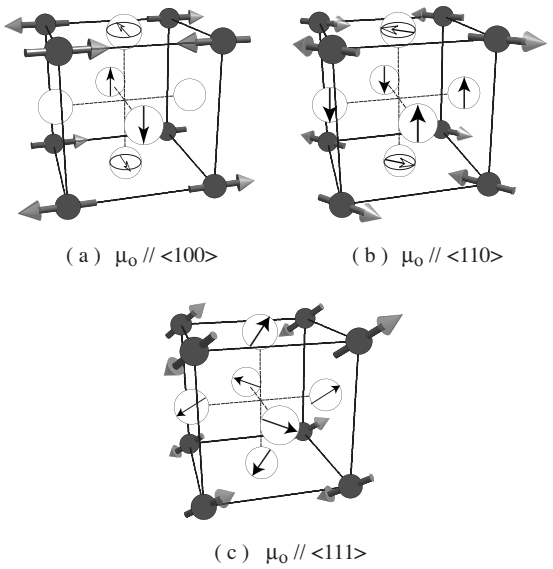

FIG. 8. Illustrations of induced magnetic moments on In sites for the cases where the U moments (μ_o) are parallel to (a) $\langle 100 \rangle$, (b) $\langle 110 \rangle$, and (c) $\langle 111 \rangle$.

These simulation curves are calculated numerically as follows. In order to calculate resonant frequencies and intensities with reasonable fixed parameters, numerical diagonalization of the effective Hamiltonian matrix, including Zeeman and quadrupole terms, is performed for each In site. Then, a simulated spectrum is obtained by convolution of a Gaussian function with a natural width. As a fixed parameter, $\nu_Q = 11.8$ MHz is used, which is obtained experimentally just above T_N. In the case of $\mu_o \| \langle 110 \rangle$, the $H_i^{(\|,\perp)}$ are used only as fitting parameters, and in the case of $\mu_o \| \langle 111 \rangle$, H_i and θ are used only as fitting parameters.

As shown in Fig. 6(b), in the case of $\langle 111 \rangle$, the multivalley structure can be reproduced to some extent with $H_i \sim 3-6$ kOe and $\theta \sim 50° - 60°$. Even if H_i and θ are varied from these values, the fit cannot be improved significantly. It is also noted that the case of μ_o along $\langle 111 \rangle$ with type-II AF structure has been indicated to be unstable for UIn_3 by *ab initio* calculations.[22]

On the other hand, the best fit to the experimental data can be obtained with $\mu_o \| \langle 110 \rangle$ when $H_i^{(\|)} = 32.5$ kOe and $H_i^{(\perp)} = 21.4$ kOe. The multivalley structure can be well reproduced as shown in Fig. 6(a), although part of the spectrum deviates slightly from the simulation around 40–60 MHz. This comes from certain In sites feeling a parallel hyperfine field $H_i^{(\|)}$, as denoted by the thin lines in Fig. 6(a). Here, it must be noted that the experimental spectrum in the range of 10–40 MHz is well reproduced by In sites with $H_i^{(\perp)}$, as denoted by thick lines in Fig. 6(a). Thus, it seems that some fraction of In sites is subjected to a hyperfine field with $\theta = 90°$. As for the deviation in Fig. 6(a) from the simulated spectrum around 40–60 MHz, this may be due to microscopic magnetic domains which have been suggested to

exist in the related antiferromagnet UGa_3.[12] In addition, for better fitting, a variation in ν_Q may be valid since such a change in the EFG in the ordered state is often observed in antiferromagnets. For simplicity we do not pursue this possibility here.

Based on the foregoing considerations, moment orientations along $\langle 111\rangle$ or $\langle 100\rangle$ seem to be only remotely possible, while $\langle 110\rangle$ direction is found to be the most probable direction for the ordered moments among the possible orientations according to the crystallographical axes. Finally, it should be mentioned about the more general cases, i.e., the other possibilities such as $\mu_o \| \langle uvw\rangle$, $\langle 11w\rangle$, or $\langle uv0\rangle$, where $u, v, w \neq 0, 1$. The possibilities of $\mu_o \| \langle uvw\rangle$ and $\langle 11w\rangle$ may be ruled out since the hyperfine fields on In sites would not be perpendicular to principal axis of EFG. As mentioned already, the hyperfine fields on the some portion of In sites are suggested to be $\theta = 90°$ experimentally. However, the rest situation of $\mu_o \| \langle uv0\rangle$ $(u \neq v)$ cannot be ruled out at the present since the In sites would feel the hyperfine fields with $\theta = 90°$ even in this case.

V. SUMMARY

We have carried out an ^{115}In NMR/NQR study on the cubic antiferromagnet UIn_3. In the paramagnetic state, the hyperfine parameters ν_Q and K have been estimated from NMR powder patterns. The hyperfine coupling constant $A_\perp$ so obtained is very similar to that of the heavy fermion system USn_3. The NQR relaxation rates $1/T_1$ show temperature-independent behavior at temperatures above T_N, while showing critical slowing down near T_N. This result indicates that 5*f* electrons of UIn_3 have a strongly localized nature.

As for the AF state in UIn_3, the ^{115}In NMR spectrum under zero field has been observed at temperatures down to 4 K. On the basis of symmetry analysis and assuming that the ordered moment lies along a $\langle 110\rangle$ axis, calculated curves are found to reproduce the multivalley structure of the NMR spectrum. Thus, a $\langle 110\rangle$ orientation is highly plausible for the AF-ordered moment in UIn_3, among the possible orientations according to the crystallographical axes.

Our study is important as complimentary information to the neutron and the PAC experiments to elucidate the AF state in UIn_3. In addition, it is also helpful for understanding of Fermi surfaces in UIn_3 since the observed dHvA oscillations in the AF state of this system[16] may be interpreted with a 5*f* localized model having the AF moment along a $\langle 110\rangle$ axis.

ACKNOWLEDGMENTS

We would like to thank E. Yamamoto and T. D. Matsuda for experimental support and encouragement. We also would like to thank R. E. Walstedt for helpful suggestions and stimulating discussions. This research was partially supported by the Ministry of Education, Culture, Sports and Science and Technology, Grant-in-Aid for Scientific Research (C) (Grant No. 19540385), 2008.

*sakai.hironori@jaea.go.jp
†Present address: I. Physik. Institut, Georg-August-Universität Göttingen, D-37077, Göttingen, Germany.
‡Present address: INAC/SPSMS, CEA-Grenoble, 17 rue des Martyrs, 38054 Genoble, France.

[1] M. R. Norman, S. D. Bader, and H. A. Kierstead, Phys. Rev. B **33**, 8035 (1986).
[2] D. Kaczorowski, J. Phys. Soc. Jpn. **75**, 68 (2006).
[3] A. J. Arko and D. D. Koelling, Phys. Rev. B **17**, 3104 (1978).
[4] Y. Tokiwa *et al.*, J. Phys. Soc. Jpn. **69**, 1105 (2000).
[5] D. Aoki *et al.*, J. Phys. Soc. Jpn. **69**, 2609 (2000).
[6] S. Kambe, H. Sakai, Y. Tokunaga, T. D. Matsuda, Y. Haga, H. Chudo, and R. E. Walstedt, Phys. Rev. B **77**, 134418 (2008).
[7] A. Murasik, J. Leciejewicz, S. Ligenza, and A. Zygmunt, Phys. Status Solidi A **23**, K147 (1974).
[8] A. C. Lawson, A. Williams, J. L. Smith, P. A. Seeger, J. A. Goldstone, J. A. O'Rourke, and Z. Fisk, J. Magn. Magn. Mater. **50**, 83 (1985).
[9] D. Kaczorowski, R. Troć, D. Badurski, A. Böhm, L. Shlyk, and F. Steglich, Phys. Rev. B **48**, 16425 (1993).
[10] P. Dervenagas, D. Kaczorowski, F. Bourdarot, P. Burlet, A. Czopnik, and G. H. Lander, Physica B **269**, 368 (1999).
[11] D. Aoki *et al.*, J. Phys. Soc. Jpn. **70**, 538 (2001).
[12] S. Kambe, R. E. Walstedt, H. Sakai, Y. Tokunaga, T. D. Matsuda, Y. Haga, and Y. Ōnuki, Phys. Rev. B **72**, 184437 (2005).
[13] A. Murasik, J. Leciejewicz, S. Ligenza, and A. Misiuk, Phys. Status Solidi A **20**, 395 (1973).
[14] J. Leciejewicz and A. Misiuk, Phys. Status Solidi A **13**, K79 (1972).
[15] Y. Haga *et al.*, J. Phys. Soc. Jpn. **71**, 2019 (2002).
[16] Y. Tokiwa, D. Aoki, Y. Haga, E. Yamamoto, S. Ikeda, R. Settai, A. Nakamura, and Y. Ōnuki, J. Phys. Soc. Jpn. **70**, 3326 (2001).
[17] L. Asch, G. M. Kalvius, A. Kratzer, and F. J. Litterst, Hyperfine Interact. **85**, 193 (1994).
[18] Y. Kratzer, H. H. Klauß, S. Zwirner, G. M. Kalvius, and J. C. Spirlet, Hyperfine Interact. **85**, 431 (1994).
[19] A. Kratzer, C. Schopf, G. M. Kalvius, H. H. Klauß, S. Zwirner, and J. C. Spirlet, Hyperfine Interact. **104**, 181 (1997).
[20] S. Zwirner, J. C. Spirlet, K. H. Münch, A. Kratzer, L. Asch, and G. M. Kalvius, Physica B **186-188**, 798 (1993).
[21] T. Yuen, C. L. Lin, J. E. Crow, and N. Bykovetz, J. Magn. Magn. Mater. **109**, 98 (1992).
[22] S. Demuynck, L. Sandratskii, S. Cottenier, J. Meersschaut, and M. Rots, J. Phys.: Condens. Matter **12**, 4629 (2000).
[23] D. E. MacLaughlin, J. D. Williamson, and J. Butterworth, Phys. Rev. B **4**, 60 (1971).
[24] R. R. Hewitt and T. T. Taylor, Phys. Rev. **125**, 524 (1962).
[25] N. J. Curro, B. L. Young, J. Schmalian, and D. Pines, Phys. Rev. B **70**, 235117 (2004).
[26] N. J. Curro, B. Simovic, P. C. Hammel, P. G. Pagliuso, J. L. Sarrao, J. D. Thompson, and G. B. Martins, Phys. Rev. B **64**, 180514(R) (2001).
[27] T. Ohama, H. Yasuoka, D. Mandrus, Z. Fisk, and J. Smith, J. Phys. Soc. Jpn. **64**, 2628 (1995).
[28] S. Takagi, H. Muraoka, T. D. Matsuda, Y. Haga, S. Kambe, R. E. Walstedt, E. Yamamoto, and Y. Ōnuki, J. Phys. Soc. Jpn. **73**, 469 (2004).
[29] T. Moriya, Prog. Theor. Phys. **16**, 23,641 (1956).